Check for updates

Making photochemistry scalable – an operationally simple falling film looping photoreactor†

Shibu Naskar,‡[a] Daniel Kowalczyk, [iD] ‡[b] Susital Mal,[a] Subrata Das,*[a] Debabrata Mandal,[c] Prakash Kumar[c] and Dirk Ziegenbalg [iD] *[b]

Visible light-driven organic transformations have become very widespread due to their energy efficiency, process simplicity and high selectivity. Since photoreactions occur in a wide range of wavelengths and conditions, designing a specific reactor is very strenuous and challenging. Hence, different reactor types are required to meet the different demands of photoreactions but suited scale-up strategies do not yet exist for relevant reactor types. Crucial links for the scale-up process are still missing. Ideally, a scale-up process should be performed within the same type of reactor ensuring comparable reaction conditions. To resolve this issue, a new looping photoreactor was designed and manufactured that recirculates the reaction mixture and generates a falling film within the photoreactor. The reactor concept allows small-scale photoreactions to be carried out on a laboratory scale and demonstrates the scalability of the reactor concept without major changes to the reaction conditions up to productivities on the 1.7 kg per day scale.

Introduction

In recent years, visible light-driven organic synthesis has become very popular among researchers.[1–7] Nevertheless, the underlying potential of photochemical organic synthesis for industrial application cannot be revealed without suited photoreactor scale-up strategies. Ideally, a reactor should therefore be scalable in a bottom-up approach, starting from laboratory conditions. Photoreactions can be performed either in batch or in flow. Batch stirred tank reactors (BSTRs) like glass flasks equipped with stirring bars are well-suited for initial experimentation. These reactors are usually less complex from both operational and technological perspectives and are therefore less cost intensive. Especially for reactor volumes from the μL to low mL range, the inherent disadvantages of BSTRs, like light attenuation or problems of heat- and mass-transfer, are less pronounced. Elliott *et al.*

showed that if key reaction parameters are matched, then the productivity of a flow reactor varies little with respect to the batch case, making both irradiation modes equally important for synthetic photochemistry.[8] Taking the trifluoromethylation of *N*-Boc-pyrrole as an example, simple scaling of the reaction batch from 18.3 g to 100 g using the same batch photoreactor and the same light source led to a significant drop in the product yield by around 39% together with an increase of reaction time (batch reference: 15 h; scale-up: 62 h). This exemplifies the crucial influence of relative photon availability per substrate molecule within a photochemical reaction. Utilization of a wound capillary as a continuous flow photoreactor yielded 71% product using a 20 g substrate with the reaction time halved (batch reference: 15 h; capillary: ~7 h).[9] In contrast, the integrated batch scale photoreactor designed by Davies and MacMillan enables acceleration of selected photocatalytic reactions on a laboratory scale.[10] The choice of one operation mode over the other should therefore be based on the particular experimental requirements. In the Hitchhiker's Guide to Flow Chemistry, Plutschack *et al.* answer the question if flow is the answer to the ultimate question of life, the universe, and everything with a clear no and provide a simple scheme for the assessment whether flow or batch conditions should be used for a certain reaction.[11] In fact, flow photochemistry in microreactors can provide many advantages over batch processes such as improved mass- and heat-transfer, fewer safety hazards, higher efficiencies in terms of yields and reaction times, high surface-to-volume ratios and thorough

[a] *Department of Chemistry, National Institute of Technology Patna, Bihar 800005, India. E-mail: subratad@nitp.ac.in*

[b] *Institute of Chemical Engineering, Ulm University, Albert-Einstein-Allee 11, 89081 Ulm, Germany. E-mail: dirk.ziegenbalg@uni-ulm.de*

[c] *National Institute of Pharmaceutical Education and Research Hajipur, Bihar 844102, India*

† Electronic supplementary information (ESI) available: Experimental procedure and measurement data for the falling film looping photoreactor (PDF). Flow within batch process demonstration video (mp4). Falling film flow at the inner wall (mp4). Different glassware and integrated light assembly demonstration video (mp4). Reaction set up demonstration video (mp4). See DOI: https://doi.org/10.1039/d3re00107e

‡ These authors contributed equally.

This journal is © The Royal Society of Chemistry 2023

React. Chem. Eng., 2023, **8**, 2211–2222 | **2211**

irradiation.[12] Since most photoreactions depend on the absorption of photons in stoichiometric amounts, photophysical limitations such as the exponential decay of the photon flux with the depth of the reaction vessel, as described by the Beer–Lambert law, change the availability of photons as a reagent for the photoreaction. In addition, capillary milli-photoreactors show significantly higher space time yields (STYs) than conventional batch reactors.[13,14] Despite these advantages, scaling of continuous micro- and milli-flow chemistry has its own challenges and limitations. The capacity of a flow reactor can be increased by increasing the volumetric flow rate, which also requires an increase of the reactor volume to maintain the residence/reaction time. The volume scaling of tubular reactors involves the parameters summarized in eqn (1).

$$V = \frac{\pi}{4} \cdot N \cdot L \cdot D^2 \tag{1}$$

The volume V of the tubular reactor can be increased by the number N of parallelized channels (internal numbering-up) or individual reactors (external numbering-up), the length of the tube L or its diameter D. Internal numbering-up has challenges towards flow equipartition, while external numbering-up has the disadvantage of high investment costs since individual equipment (*e.g.*, pumps, mass flow controllers) must be used for each reactor. Even though flow equipartition can be characterized experimentally and theoretically, fabrication imperfections, operational problems (reactor fouling and stuck gas bubbles) or clogging due to the precipitation of solid materials can result in flow maldistribution.[15] Sizing-up in length keeps a beneficial surface-to-volume ratio but leads to an increasing pressure drop. A larger diameter of a capillary decreases the surface-to-volume ratio, thus raising the problem of light attenuation.[16] Since conventional scale-up or numbering-up is not always fully suited for industrial needs, a combination of both is more realistic.[15] Although scaled-up capillary and tubular flow photoreactors with productivities (reference time: 24 h) on the high gram to single digit kilogram scale exist, this technology has not been used for ton-scale photochemical synthesis yet.[17–19] A noteworthy example for a scaled-up continuous stirred-tank reactor (CSTR) type photoreactor is the continuously operated laser driven photoreactor presented by Harper *et al.* for photocatalyzed C–N coupling with productivities of 1.8 kg d^{-1}.[20] Considering the requirements of gas–liquid photoreactions such as high liquid-to-gas contact surfaces, high shear reactors such as rotating disk reactors and vortex reactors must be mentioned as intensified and scalable photoreactors.[21,22] For the latter, Lee *et al.* showed the scalability of the concept by a factor of 300 for gas–liquid visible light induced photo-oxidation and a factor of 10 for UV-induced [2 + 2] cycloaddition with productivities of up to 7.45 kg d^{-1}.[23] Besides tubular milli- and micro-scale reactors, CSTRs and high shear photoreactors, falling thin film reactors represent another type of continuous reactor that exhibits great potential for the application within

synthetic photochemistry. The falling film microreactor developed by the Fraunhofer Institute for Microengineering and Microsystems in Mainz, with liquid film thicknesses of a few hundreds of micrometers and large interfacial areas of up to 20 000 m^2 m^{-3}, was applied for various chemical reactions including photochemical chlorination.[24] Besides this, the successful immobilization of TiO$_2$ as a heterogeneous catalyst for C–H arylation of heteroarenes with yields up to 99% was demonstrated by Fabry *et al.* within a microstructured falling film reactor, emphasizing another advantage of the falling film photoreactor concept in the context of the application of heterogeneous catalysts.[25] A larger annular falling film photoreactor with film thicknesses <1 mm has been shown to be an effective tool for the continuous photochemical prevulcanization of natural rubber.[26] Advanced oxidation processes (AOPs) for the degradation of organic compounds in wastewater are further larger-scale application for falling film photoreactors.[27–30] The design characteristics of falling film photoreactors for effective scale-up by simple proportional resizing are:

1. Small film thickness that
   - Minimizes the light attenuation effect and
   - Counteracts heat and mass transfer issues.

2. High surface-to-volume ratios with a tunable surface-to-volume ratio for optimal photon utilization.

3. Relatively simple operation by distribution of the reaction solution using spillways.

Despite the mentioned advantages of falling film reactors in the context of scale-up within photochemistry, no extensive studies on the scaling process of a specific falling film photoreactor concept starting from the mg lab-scale have been published to date. A falling film looping photoreactor was developed with the aim of bridging the gap between the small- and larger-scale. The main objectives while designing the falling film looping photoreactor were:

- Accelerate photoreactions compared to the batch case,
- Enable reaction optimization on a small scale, and
- Enable scalability starting from small scale laboratory conditions to a scaled photoreactor version with similar efficiency by
  - Counteracting light attenuation,
  - Ensuring comparable optical characteristics along the different scales of the photoreactors,
  - Counteracting mass transport limitations and
  - Counteracting heat transfer limitations.

Through this article, the scalability of the falling film looping photoreactor design is demonstrated together with crucial contemplation on the scale-up process in the context of comparable photonic characteristics and reaction conditions by three photoreactor models increasing in size. The photoreactor concept was validated using two literature-known visible light driven photoreactions, the benzylic bromination of toluene using *N*-bromosuccinimide (NBS) (reaction 1) and the trifluoromethylation of 1,3,5-trimethoxybenzene using the Langlois reagent (reaction 2). The results are evaluated based on the framework for

standardized reporting of data within light-driven catalysis presented by Ziegenbalg *et al.*[31]

Falling film looping photoreactor concept

The main objective was to design a scalable falling film looping photoreactor concept that allows both reaction optimization at the laboratory level (mg scale) and consecutive scale-up of the performed photoreaction using different proportionally scaled versions of the photoreactor. A depiction of the photoreactor and its components is shown in Fig. 1.

The developed photoreactor consists of the following five main modules:

a) Pump module:
- Peristaltic pump with an 8 mm internal diameter silicon tube
- Little dark volume inside the silicon tubing

b) Irradiation module:
- Precise positioning of LEDs for different reactor sizes (see the ESI† for details)
- Number of LEDs scaled with the outer surface of the photoreactor glassware

c) Controller module:
- Current and voltage setting (LED power)
- Flow rate setting
- Magnetic stirrer setting
- Fan speed setting

d) Case module:
- Optical protection from the irradiation module

e) Fan plus cooling coil at the back side of the irradiation chamber, exhaust fan at the top

f) Magnetic stirrer

g) Reactor module:
- Cylindrical glassware with a reservoir for the reaction solution at the bottom and spillway for distribution of the reaction solution at the top

- Loop operation using a peristaltic pump (recycling of reaction solution)
- Batch operation mode without looping possible
- Operation under an inert atmosphere possible

The corresponding irradiation module is equipped with the reactor module and placed within the case module. The reactor is connected through silicon tubing to the peristaltic pump. The schematic working principle of the reactor module is depicted in Fig. 1g. During reactor operation, the reaction solution is continuously pumped from the reservoir at the bottom of the glassware to the distributor at the top and distributed in a thin film using a spillway. The reaction solution is irradiated by an LED array at the outer surface of the glassware along the falling film. A picture of the smallest glassware used is depicted in the figure as well. For a detailed description of the photoreactor setup see Fig. S1.†

Scale-up concept

The general scale-up strategy considers that the photon-to-reactant ratio must be kept constant, independent of the size of the reactor. For a falling-film setup, the film thickness can be assumed constant. Thus, a change in the film area proportionally changes the liquid film volume. With this, a constant photon-to-reactant ratio can be realized when the irradiance (or photon fluence rate) incident on the falling film is kept constant. By scaling the film area and at the same time maintaining the irradiance, the total photon flux is increased linearly with the irradiated volume and thus the capacity.

Three different sizes of the falling film looping photoreactor were manufactured for a three step scale-up procedure. The smallest reactor module ($1 \times A$) with a diameter of 25 mm and a height of 100 mm of the cylindrical part of the reactor possessed a wetted area of $A = 78.5$ cm^2 and was scaled by factors of 2 and 4, leading to reactors $2 \times A$ ($A = 179.1$ cm^2) for the intermediate and $4 \times A$ ($A = 314.2$ cm^2) for the largest scale, respectively. Depictions of the different reactor modules are shown in Fig. 2a. Together with the irradiated surface, the number of applied LEDs was scaled to ensure similar irradiance for the different reactor sizes (see
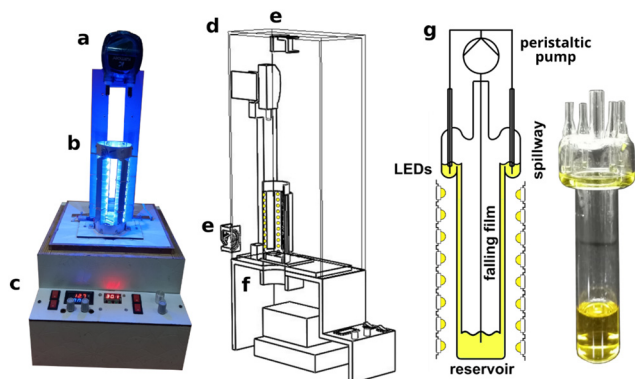

Fig. 1 Falling film looping photoreactor setup consisting of a peristaltic pump (a), an irradiation module (b), a control unit (c), reactor casing (d), fans (e), a magnetic stirrer (f) and photoreactor glassware with a spillway and working principle of the falling film looping photoreactor (g).
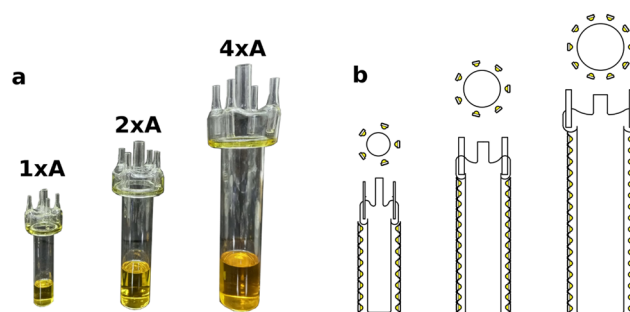

Fig. 2 Different sizes of the falling film looping photoreactor (a), smallest ($1 \times A$), intermediate ($2 \times A$) and largest ($4 \times A$) scale. Schematic depiction of the LED assembly for the different sized reactors (b).

Table 1 Optical properties of the $1 \times A$, $2 \times A$ and $4 \times A$ falling film looping photoreactors

Reactor module	Wetted surface A/cm^2	Number of LEDs	Electrical current/A	Current per LED/mA	Total photon flux $q_{emitted}$/µmol s^{-1}	Total radiant power P/W	Irradiance E/mW cm^2
$1 \times A$	78.5	40	1	71–77	21	4.71	60.1
		40	2	143–154	38	8.56	109.0
		40	2.5	179–192	46	10.32	131.4
$2 \times A$	179.1	91	5	177–183	102	22.81	127.4
$4 \times A$	314.2	160	10	185–189	185	41.27	131.4

Table 1, reference case: E = 60.1 mW cm^{-2}). The schematic depiction of the irradiation modules can be seen in Fig. 2b. Details of the irradiation setup are presented in Fig. S2.† To ensure a similar behaviour of the falling film for the different reactor sizes, applied flow rates were tuned to maintain the same space velocity s:

$$s = \frac{\dot{V}}{V} \tag{2}$$

representing the number of cycles per time by relating the applied flow rate $\dot{V}$ to the volume of the reaction solution V.

Photonic characterization

As a basis for the scale-up, the photonic properties of the used LEDs were experimentally determined. The emitted optical power of the LEDs was found to increase linearly with the applied electrical current, even though a slight deviation from the linear correlation was found for higher currents (see Fig. S26†). The emission spectrum and the geometrical emission properties of the light sources are depicted in the ESI† (see Fig. S25 and S29). A viewing angle of about 60° was measured for the light source. The optical properties of the different reactor modules are summarized in Table 1. In terms of total radiant power, a range from 4.7 W to 41.3 W, equal to photon fluxes of 21 µmol s^{-1} to 185 µmol s^{-1}, can be realized with the used setups. This enables a potential scale-up by a factor of 9.

Photoreactions

Performance indicators

The choice of suited performance indicators plays a crucial role in the comparison of photochemical systems. Especially if different photoreactors are evaluated concerning their performance, the right choice of metrics is essential for the comparison of experimental results.[31] A comparison can be based on the converted molar amount of a consumed educt or produced substance Δn. Normalization to the initial molar amount of the educt n_{educt,t_0} or the theoretical maximum molar amount of the product $n_{product,max}$ results in the conversion X or the product yield Y shown in eqn (3) and (4), respectively.

$$X = \frac{n_{educt,t}}{n_{educt,t_0}} \quad [X] = 1 \tag{3}$$

$$Y = \frac{n_{product,t}}{n_{educt,t_0} \cdot \frac{|v_{product}|}{|v_{educt}|}} \quad [Y] = 1 \tag{4}$$

v_i represents the stoichiometric coefficient for species i. Δn can also be normalized with respect to the reaction time Δt, the reaction volume V and the photon flux present at a specific place within the photoreactor.[32] If the normalization is based on the reaction time Δt, the corresponding metric results in the reaction rate, as depicted in eqn (5).

$$r = \frac{\Delta n \text{ (educt or product)}}{\Delta t} \tag{5}$$

If the normalization is additionally performed with respect to V, the resulting performance indicator can be defined as a space–time-conversion (STC) or space–time-yield (STY) shown in eqn (6) and (7).

$$STC = \frac{\Delta n \text{ (educt)}}{\Delta t \cdot V \text{ (reaction volume)}} \tag{6}$$

$$STY = \frac{\Delta n \text{ (product)}}{\Delta t \cdot V \text{ (reaction volume)}} \tag{7}$$

Photoreactions are often limited by the photon flux emitted by a light source $q_{emitted}$. The normalization of the reaction rate to $q_{emitted}$ leads to the external photonic efficiency (ξ_{ext}) defined in eqn (8).[33]

$$\xi_{ext} = \frac{r}{q_{emitted}} \tag{8}$$

Assessment of the average film thickness

An experimental assessment of the film thickness is difficult. It strongly depends on the flow regime and changes along the height of the falling film reactor. For a theoretical evaluation, the Reynolds number Re can be used to assess the flow regime:[34]

$$Re = \frac{\dot{m}}{U \cdot \eta}, \tag{9}$$

with the mass flow rate $\dot{m}$ in the falling film reactor, the film width U (corresponding to the circumference of the reactor) and the dynamic viscosity η of the used solvent. Three main flow regimes can be distinct from each other: i) purely laminar smooth films and stable wavy laminar films (Re ≤ 75), ii) wavy films in the transition region to turbulent flow (75 ≥ Re ≤ 400) and iii) fully turbulent flow (Re ≥ 400).[34] The average film thickness of wavy laminar films $\bar{\delta}_{lam,wav}$ can be calculated using the kinematic viscosity v and the gravitational acceleration g:[34]

2214 | *React. Chem. Eng.*, 2023, **8**, 2211–2222

This journal is © The Royal Society of Chemistry 2023

$$\bar{\delta}_{lam,wav} = \left(\frac{2.4 \cdot v^2}{g}\right)^{1/3} \cdot Re^{1/3}. \quad (10)$$

For a turbulent flow regime, the average film thickness $\bar{\delta}_{turb}$ can be calculated as follows:[34]

$$\bar{\delta}_{turb} = 0.302 \cdot \left(\frac{3 \cdot v^2}{g}\right)^{1/3} \cdot Re^{8/15}. \quad (11)$$

A dynamic viscosity of $\eta = 0.34627$ mPa s for the reaction solution used for reaction 1 was estimated under the assumption of a binary mixture of toluene in acetonitrile (for more information see Fig. S6†).[35] Calculated Re, $\bar{\delta}_{lam,wav}$ and $\bar{\delta}_{turb}$ for the $1 \times A$, $2 \times A$ and $4 \times A$ reactor modules at different flow rates are summarized in Table 2.

Table 2 Calculated, $\bar{\delta}_{lam,wav}$ and $\bar{\delta}_{turb}$ for the $1 \times A$, $2 \times A$ and $4 \times A$ reactor modules at different flow rates

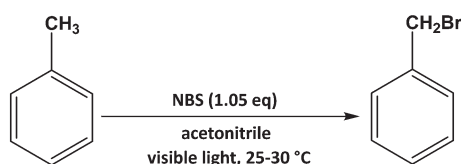| Reactor module	Flow rate/mL min^{-1}	Re/1	$\bar{\delta}_{lam,wav}$/µm	$\bar{\delta}_{turb}$/µm
$1 \times A$	150	72	163	125
$1 \times A$	300	143	206	181
$2 \times A$	75	24	113	69
$2 \times A$	250	79	169	131
$2 \times A$	500	157	212	190
$2 \times A$	750	236	243	236
$4 \times A$	1500	359	280	295

Fig. 3 Reaction scheme of the benzylic bromination of toluene in acetonitrile using *N*-bromosuccinimide.

Reaction 1: benzylic bromination of toluene using *N*-bromosuccinimide

Radical bromination using NBS as a mild and user-friendly reagent finds wide application as an alternative to the utilization of hazardous bromine as a reagent (see Fig. 3).[36] The radical NBS reaction can be initiated by light within the UV and visible region with and without catalysts.[37–39] Cantillo *et al.* reported the bromination reaction of toluene to benzyl bromide using NBS in acetonitrile in continuous flow in a capillary photoreactor, using various light sources.[40] Therefore, this reaction was chosen as the first benchmark reaction for optimization and consecutive scale-up.

Different photon fluxes (21 µmol s^{-1}, 38 µmol s^{-1}, 46 µmol s^{-1}), as shown in Table 1, were studied on the 0.46 g scale (500 mM toluene in acetonitrile) in the $1 \times A$ module. For the experiments, a reaction volume of 10 mL together with a space velocity $s = 15$ min^{-1} were used. The corresponding time-dependent product yields and STYs are depicted in Fig. 4 and Table 3. For a total photon flux of 21 µmol s^{-1}, reaction times of 480–600 s were required to achieve the desired yield of approximately 92%. An increase of the photon flux to 38 µmol s^{-1} and 46 µmol s^{-1} led to a reduction of the reaction time to 360–480 s and 240–360 s, respectively. With this, a linear correlation between the time to reach a given yield and the photon-to-reagent ratio is observed. This corresponds to a decrease of the reaction time by around 50%, correlating well with the approximately doubled photon flux. Analogous to this, the maximum STYs (see Fig. 4 right) increased according to the increase in the photon-to-reagent ratio.

Different volumes V of 10 mL, 20 mL and 30 mL (500 mM toluene in acetonitrile) corresponding to specific surface

Table 3 r and ξ_{ext} for the bromination reaction of toluene at $\Delta t = 0$–120 s and $\Delta t = 120$–240 s dependent on $q_{emitted}$

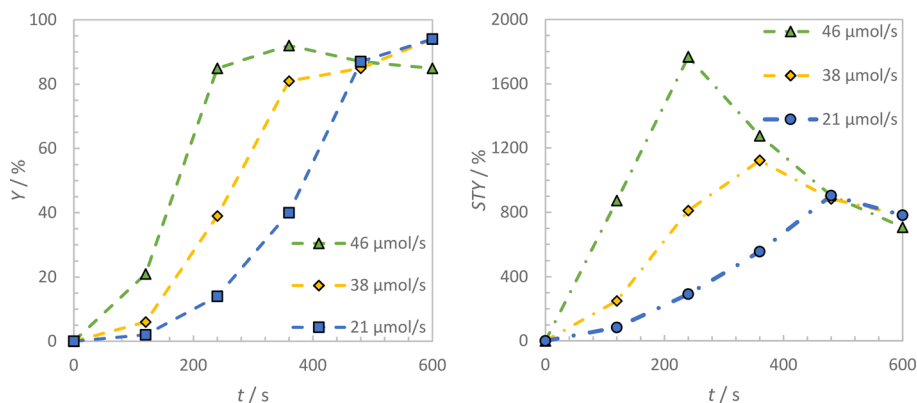| $q_{emitted}$/µmol s^{-1}	Δt/s	r/µmol s^{-1}	ξ_{ext}/1	Δt/s	r/µmol s^{-1}	ξ_{ext}/1
21	0–120	1	0.04	120–240	5	0.24
38		2	0.07		14	0.36
46		9	0.19		27	0.58

Fig. 4 Time dependent product yields and STYs for the bromination of toluene in dependence of the total photon flux.
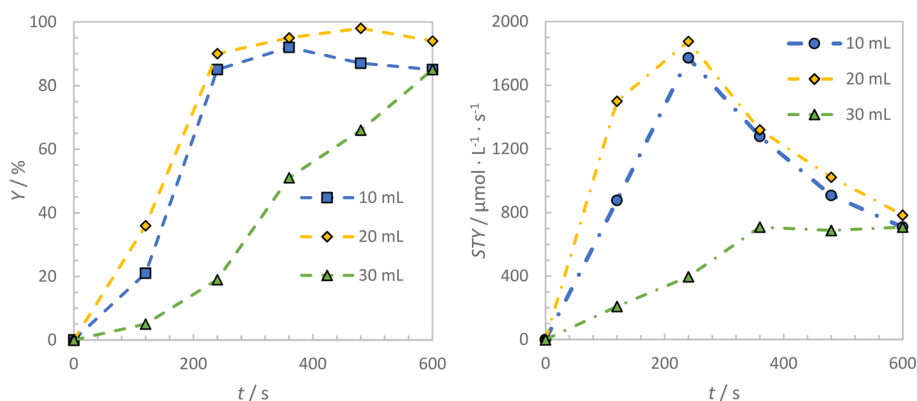
This journal is © The Royal Society of Chemistry 2023

React. Chem. Eng., 2023, **8**, 2211–2222 | **2215**

Table 4 r and ξ_{ext} for the bromination reaction of toluene at Δt = 0–120 s and Δt = 120–240 s dependent on V

V/mL	Δt/s	r/µmol s^{-1}	ξ_{ext}/1	Δt/s	r/µmol s^{-1}	ξ_{ext}/1
10	0–120	9	0.19	120–240	27	0.58
20		30	0.65		45	0.97
30		9	0.14		18	0.38

areas of 785 m^2 m^{-3}, 393 m^2 m^{-3} and 262 m^2 m^{-3} were investigated with a space velocity of s = 15 min^{-1} and a photon flux of 102 µmol s^{-1} in the 2 × A module (see Table 4). Increasing the reaction volume from 10 mL to 20 mL led to an increase of r (Δt = 120–240 s) from 27 µmol s^{-1} to 45 µmol s^{-1}, corresponding to an increase of approximately 57%. This corresponds well with the resulting ξ_{ext} of 0.58 and 0.97. With respect to the yield and STY, the reaction performs very similar for the 10 mL and 20 mL scale. In contrast, V = 30 mL led to a significant decrease in r and ξ_{ext} (18 µmol s^{-1}, 0.38) (see Fig. 5). A similar trend can be

observed for the peak STY, where a decrease by around 62% from 20 mL to 30 mL is visible. These results indicate that a larger volume causes unfavorable reaction conditions. The increasing volume in the lower part of the reactor might be detrimental, leading to strong intensity gradients and thus uncontrolled decomposition of NBS. The formed bromine radicals might react in an undesired manner.

The effect of the falling film was evaluated by comparing the reactor in falling film looping mode and batch mode without a falling film for a reaction volume of 20 mL (500 mM toluene in acetonitrile) in the 1 × A module. For operation in looping mode, a space velocity of s = 15 min^{-1} was applied. During batch operation, no looping was applied. Instead, the reaction solution was actively mixed using a magnetic stirrer. When looping was applied and thus a falling film was irradiated, an over 6-fold increase of the reaction rate r from 5 µmol s^{-1} to 30 µmol s^{-1} (Δt = 0–120 s) during the initiation period was observed in comparison to the batch case (see Table 5 and Fig. 6). This is reflected in the ξ_{ext}, increasing

Fig. 5 Time dependent product yields and STYs for the bromination of toluene in dependence of the total reaction volume.

Table 5 r and ξ_{ext} for the bromination reaction of toluene at Δt = 0–120 s and Δt = 120–240 s dependent on the operational mode of the reactor module either with or without the application of a falling film

Operational mode	Δt/s	r/µmol s^{-1}	ξ_{ext}/1	Δt/s	r/µmol s^{-1}	ξ_{ext}/1
No falling film	0–120	5	0.11	120–240	32	0.69
Falling film		30	0.65		45	0.97

Fig. 6 Time dependent product yields and STYs for the bromination of toluene with and without the application of looping.

2216 | *React. Chem. Eng.*, 2023, **8**, 2211–2222

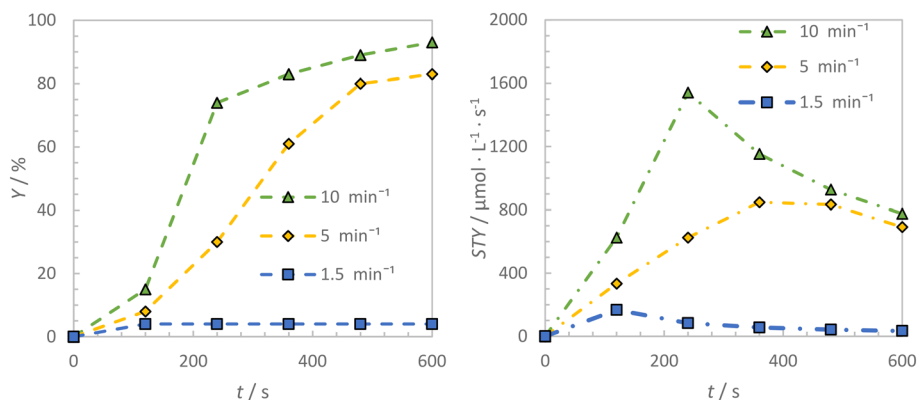This journal is © The Royal Society of Chemistry 2023

Fig. 7 Time dependent product yields and STYs for the bromination of toluene for different space velocities.

from 0.11 to 0.65 from the batch to the looping mode and can be explained by photonic limitation in the initiation phase of the radical reaction. After the initiation period, maximal r of 45 µmol s^{-1} to 32 µmol s^{-1} (Δt = 120–240 s) and ξ_{ext} of 0.97 and 0.69 were measured for both the looping and batch cases. The beneficial effect of looping can be seen as well in the STYs, resulting in a nearly two-fold increase when looping is applied (see Fig. 6). Even though the wetted surface is approximately doubled for falling film conditions, less than 2% of the incident photons (λ = 400–800 nm) are absorbed by the falling film when assuming $\bar{\delta}_{lam,wav}$ = 206 µm (for more information see Fig. S31†). In comparison, the number of absorbed photons in the reservoir part of the reactor with a diameter of 25 mm ranges from 86.1% to 5.6% over the entire spectral range (λ = 400–800 nm, for more information see Fig. S32†). This gives evidence

that the different fluid dynamic situations in the reactor are the reason for the observed performance changes.

Fig. 7 shows the influence of s on the 2 × A module for a 50 mL reaction volume (500 mM toluene in acetonitrile) and s = 1.5 min^{-1}, s = 5 min^{-1} and s = 10 min^{-1}. For irradiation, a photon flux of 102 µmol s^{-1} was applied. With an increasing s, both r and ξ_{ext} increase significantly from 8 µmol s^{-1} to 31 µmol s^{-1} and from 0.08 to 0.31 for the initiation period (Δt = 0–120 s), respectively (see Table 6). This trend gets even more pronounced in the subsequent period (Δt = 120–240 s), where r and ξ_{ext} increase from ~0 µmol s^{-1} to 123 µmol s^{-1} and ~0 to 1.20, respectively. For s = 1.5 min^{-1} almost no activity was found. Consequently, the STY increased by more than a factor of 9 from the lowest to the highest s.

The previously optimized reaction conditions for the 1 × A reactor module were used for scale-up from the 0.46 g-scale to the 0.92 g-scale, 2.3 g-scale and 4.6 g-scale, using the 1 × A, 1 × A, 2 × A and 4 × A reactor modules, respectively. Fig. 8 shows the results of the gradual scale-up process. Although no effect on the final product yield can be observed through the scale-up process, a drop of the STY for the largest reaction and reactor scale was

Table 6 r and ξ_{ext} for the bromination reaction of toluene at Δt = 0–120 s and Δt = 120–240 s dependent on of s

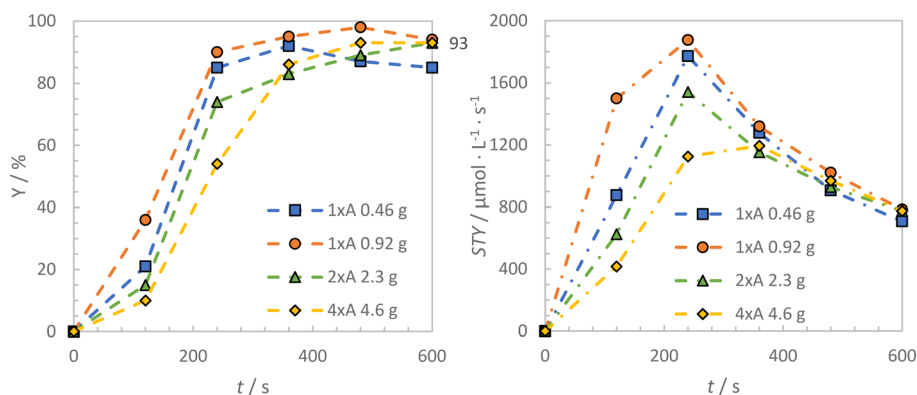| s/min^{-1}	Δt/s	r/µmol s^{-1}	ξ_{ext}/1	Δt/s	r/µmol s^{-1}	ξ_{ext}/1
1.5	0–120	8	0.08	120–240	0	0.0
5		17	0.16		46	0.45
10		31	0.31		123	1.20

Fig. 8 Time dependent product yields and calculated STYs for the bromination of toluene in dependence of the reaction scale.
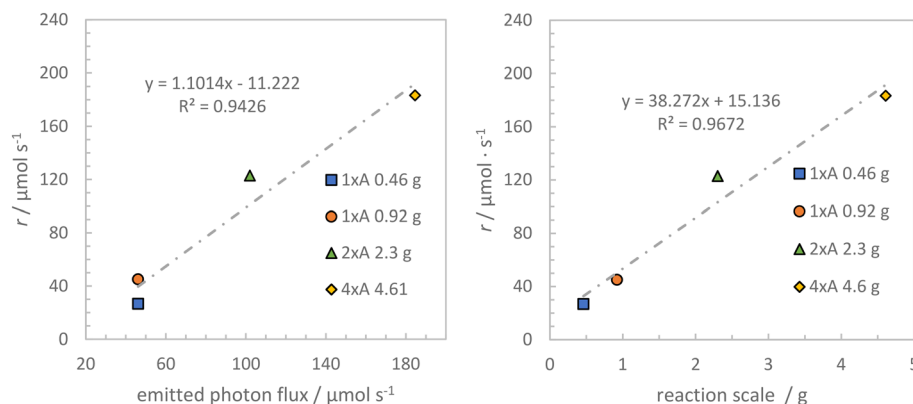
Fig. 9 Correlation of the reaction rate for the bromination reaction of toluene with the photon flux (left) and reaction scale in grams (right) for the $1 \times A$, $2 \times A$ and $4 \times A$ reactor modules at Δt = 120–240 s.

Table 7 r and ξ_{ext} for the bromination of toluene at Δt = 0–120 s and Δt = 120–240 s dependent on the reaction scale

Reaction scale/g	Δt/s	r/μmol s^{-1}	ξ_{ext}/1	Δt/s	r/μmol s^{-1}	ξ_{ext}/1
0.46	0–120	9	0.19	120–240	27	0.58
0.92		30	0.65		45	0.97
2.3		31	0.31		123	1.20
4.6		42	0.23		183	0.99

found. Reaction rates r (Δt = 120–240 s) significantly increased from 27 μmol s^{-1} to 183 μmol s^{-1} from the smallest to the largest scale, corresponding to an increase by a factor of around 7 (see Table 6). A linear increase of the reaction rates with increasing reaction scale was observed (see Fig. 9 right). This is also true for the correlation of the reaction rate with q_{emitted} (see Fig. 9 left). Nevertheless, for the smaller reaction scales (0.46 g and 0.92 g), investigated with the $1 \times A$ reactor module, obvious differences for r and ξ_{ext} were found (see Table 7). Both r and ξ_{ext} drop significantly for the smallest reaction scale, which might be explained by the influence of dark volumes in the setup, in which the reaction solution is not irradiated, *e.g.* in the tubing of the peristaltic pump. For the $1 \times A$ module, these dark volumes sum up to 3.1 mL, corresponding to 31% of the total volume of the reaction solution. Dark volumes of 3.6 mL and 4.2 mL, corresponding to 7.2% and 4.2% of the reaction solution were determined for the $2 \times A$ and the $4 \times A$ module, respectively. Thus, the influence of the dark volumes is significantly higher for the $1 \times A$ module.

Reaction: 2 trifluoromethylation with the Langlois reagent

The introduction of trifluoromethyl groups into an organic molecule is a very important class of reactions in the pharmaceutical industry.[41–43] The last few decades have witnessed several methods, reagents and substrates for the trifluoromethylation reaction.[44–49] Li *et al.* reported the visible light induced aromatic trifluoromethylation reaction by the Langlois reagent (Fig. 10).[50] For this second benchmark reaction, no optimization of the reaction conditions was conducted. Instead, a gradual scale-up from the 0.168 g-scale to the 0.336 g-scale, the 0.841 g-scale and the 1.68 g-scale was performed using the $1 \times A$, $1 \times A$, $2 \times A$ and $4 \times A$ reactor modules.

For all reaction and reactor module scales, conversions between 89–92% were observed within 1200 s (see Fig. 11). The measurements at t = 300 s were identified as outliers, caused by errors in the analytical procedure, and are therefore not considered for further calculations. Average reaction rates and ξ_{ext} were calculated for Δt = 0–1200 s depicted in Table 8.

The calculated reaction rates are significantly lower than for the first benchmark reaction but similar trends concerning the reaction rates during the reaction and reactor module scaling were observed. A linear increase of the reaction rates was found with increasing reaction scale and q_{emitted} (see Fig. 12).

These correlations (Table 8) emphasize the suitability of the chosen scaling approach and prove the applicability of the different scales of the developed falling film looping photoreactor to other photoreactions than the initially chosen benzylic bromination.
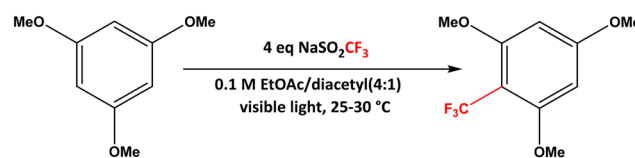

Fig. 10 Reaction scheme of trifluoromethylation of 1,3,5-trimethoxybenzene with the Langlois reagent.

2218 | *React. Chem. Eng.*, 2023, **8**, 2211–2222

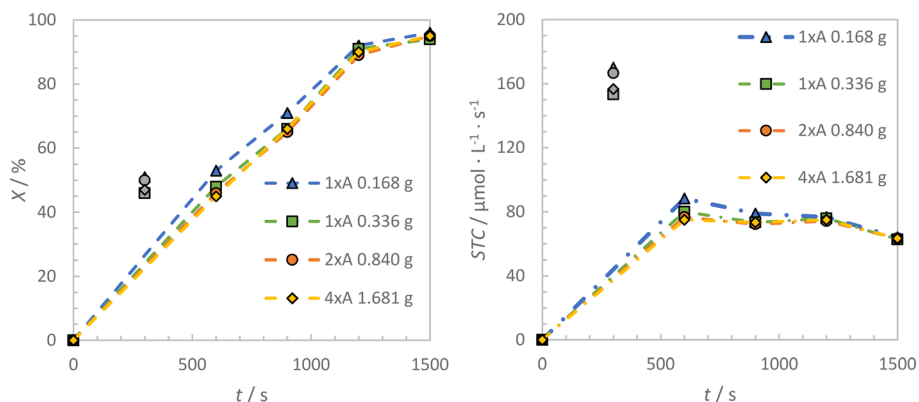This journal is © The Royal Society of Chemistry 2023

Fig. 11 Time dependent product conversions and STCs for the trifluoromethylation reaction of 1,3,5-trimethoxybenzene in dependence of the reaction scale.

Table 8 r and ξ_{ext} for the trifluoromethylation reaction of 1,3,5-trimethoxybenzene at $\Delta t = 0$–1200 s dependent on the reaction scale and utilized reactor module

Reactor module	V/mL	Reaction scale/g	X/g	X/%	Δt/s	r/μmol s^{-1}	ξ_{ext}/1
$1 \times A$	10	0.168	0.155	92	0–1200	0.64	0.01
$1 \times A$	20	0.336	0.306	91		1.25	0.03
$2 \times A$	50	0.841	0.749	89		3.17	0.03
$4 \times A$	100	1.682	1.514	90		6.33	0.03

Discussion

The main development objectives of the falling film looping photoreactor, namely the possibility to optimize reaction conditions, accelerate the reaction and increase the reactor scale, were demonstrated by two benchmark photoreactions. Optimization of the benzylic bromination of toluene for $q_{emitted}$, V and s and subsequent scale-up yielded significant increases of r and ξ_{ext}, thus increasing the overall productivity by a factor of over 63 (based on the maximum STY) from 27.86 g d^{-1} with the $1 \times A$ reactor module to 1765.10 g d^{-1} with the $4 \times A$ reactor module. Scaling the photon flux by a

factor of 10 resulted in a 6.8 times higher reaction rate. Cantillo *et al.* reported a yield of 92% for the bromination of toluene to benzyl bromide using NBS in acetonitrile (reaction scale = 0.46 g toluene, V = 13 mL acetonitrile) within 1500 s in a continuously operated capillary photoreactor irradiated with a compact fluorescent lamp (CFL, Omnilux 25 W BL Energy Saving UV-lamp).[40] These results translate into a productivity of 45.32 g d^{-1}. In the falling film looping photoreactor, the same reaction could be realized with comparable yields (~92%) in a significantly shorter reaction time of 240 s (reaction scale = 0.46 g toluene, V = 10 mL acetonitrile, $1 \times A$ reactor module, radiant power = 10.32 W). The reduction in reaction time by 84% is especially intriguing since the overlap between the absorption spectrum of the bromination agent NBS and the emission spectrum of used white LEDs is significantly lower than for a CFL emitting within the UV-range (see Fig. S25†). A comparison of the falling film looping photoreactor with the capillary reactor reported by Cantillo *et al.* in terms of productivities leads to an increase by a factor of nearly 39 for the optimized and scaled reaction performed in the falling film looping photoreactor.

For the trifluoromethylation of 1,3,5-trimethoxybenzene, a similar reduction in reaction time compared to
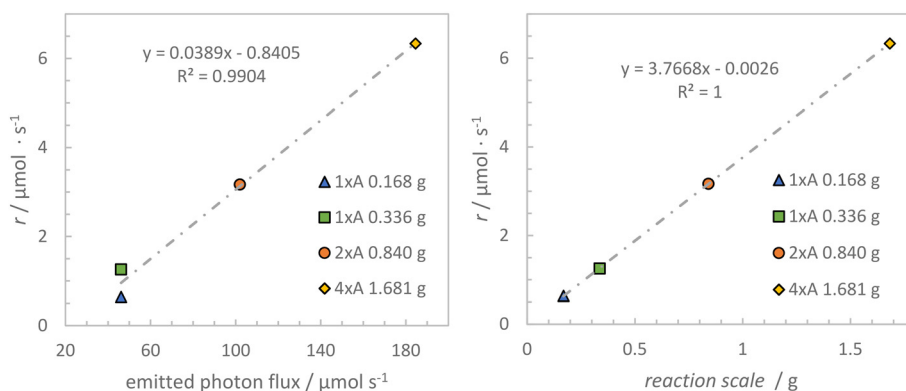

Fig. 12 Correlation of the reaction rate for the trifluoromethylation reaction of 1,3,5-trimethoxybenzene with the photon flux (left) and reaction scale in grams (right) for the $1 \times A$, $2 \times A$ and $4 \times A$ reactor modules at $\Delta t = 0$–1200 s.

This journal is © The Royal Society of Chemistry 2023

React. Chem. Eng., 2023, **8**, 2211–2222 | **2219**

published data was observed. Li *et al.* reported a 93% yield of the mono substituted trifluoromethyl derivative of 1,3,5-trimethoxybenzene with 0.1 mmol (0.0168 g) starting material after 10 hours using a 300 W xenon lamp ($\lambda > 400$ nm).[50] MacMillan and co-workers showed that the integrated photoreactor developed by them needs only 2 hours for a 70% yield using 0.25 mmol (0.0421 g) of 1,3,5-trimethoxybenzene as a starting material.[10] In the falling film looping photoreactor, conversions of 94–96% were achieved within 1500 s for the 0.168 g-scale, the 0.336 g-scale, the 0.841 g-scale and the 1.68 g-scale using the $1 \times A$, $1 \times A$, $2 \times A$ and $4 \times A$ reactor modules, respectively. Using 100 mL of the 1.68 g-scale reaction, 2.063 g of the trifluoromethyl derivative of 1,3,5-trimethoxybenzene corresponding to a yield of 87% could be isolated (for more details see the ESI†). In the reactors presented by Li *et al.* and MacMillan *et al.*, productivities of 0.053 g d^{-1} and 0.496 g d^{-1} were realized, respectively. In comparison, productivities of around 118.83 g d^{-1} (isolated $Y = 87\%$, $t = 1500$ s) were measured in this work, corresponding to an increase of the productivity by up to three orders of magnitude.

Conclusions

A falling film looping photoreactor was developed that can be scaled by one order of magnitude. Laboratory-scale reactions were successfully transferred to a larger scale with comparable efficiency. The falling film looping photoreactor concept can be used for both optimization of photoreactions and scale-up. The versatility of the developed reactor concept was demonstrated using two benchmark reactions as examples. For both reactions, significant acceleration of the reaction rates and improvement of the productivity were realized. Moreover, the presented photoreactor is easy to handle, photonically characterized and documented in a state-of-the-art fashion to ensure reproducibility of the concept. The simple yet successful scale-up strategy indicates that falling film photoreactors add significant value to the scale-up toolbox for photochemical reactions.

Experimental section

Photoreactor

All examined reactor modules were made from borosilicate glass by the central glass blowing facility of IIT Kanpur. Technical drawings of the used $1 \times A$, $2 \times A$ and $4 \times A$ reactor and irradiation modules with exact dimensions in mm are depicted in Fig. S2 of the ESI.†

Radiometry

2D radiometry. 2D radiometric measurements of the used white LEDs were performed according to the method described by Sender *et al.*[51] Electrical current dependent measurements were performed for a single LED and an LED array of 13 LEDs (for more information see Fig. S27 and

S28†). The relative 2D radiometric scans of the LED intensity were corrected to absolute optical powers using the calibration data of the white LED derived from diffuse radiometric measurements at an integrating sphere calibrated to absolute optical powers (for more information see Fig. S26†). Using the 2D intensity distribution of the measured white LED, its angle dependent normalized emission was calculated (see Fig. S30†).

Diffuse radiometric measurements using an integrating sphere. For the diffuse radiometric measurements, an integrating sphere made of optical PTFE with an inner diameter of 15 cm and a port opening of 1 cm was used. An Avantes Avaspec-ULS2048CL-EVO-RS02/17 spectrometer with a 200 μm slit Slit-200-RS coupled to the integrating sphere with an Avantes FC-UVIR600-2-ME-SMA/FC fiber optic cable was used for the relative intensity measurement of the white LEDs at constant electrical currents between 50 and 600 mA. The absolute electrical current dependent optical power of the white LED was calculated using an Energetiq EQ-99X-FC plasma light source calibrated to its optical power. The normalized emission spectrum and the electrical current dependent optical power of the measured white LED are depicted in Fig. S25 and S26.†

Photoreactions

The yield was determined by HPLC analysis.

Reaction 1. In dry glassware, *N*-bromosuccinimide (1.05 eq) was dissolved in HPLC grade acetonitrile. The glassware was put into the irradiation module. The pump was set up according to the reactor's need. Then toluene was added to the solution and mixed well. The reactor was set to the desired voltage and electrical current. The flow rate of the pump was also set as needed. 5 μL reaction mixture was taken and diluted with HPLC grade acetonitrile as needed for each sampling. The sampling was done in 2 min time intervals. The yield was measured with respect to the previously determined standard curve by using a known concentration of benzyl bromide in HPLC.

The reaction mixture collected from the reactor was taken into a round bottom flask and the solvent was evaporated under reduced pressure. The residue was shaken with 1:1 petroleum ether and diethyl ether. The precipitate was discarded and the solvent was evaporated again. This process was repeated until there was no precipitate. The product was synthesized and separated according to the reported procedure and the spectroscopic data are in agreement with the literature[40] (please see page 26 of the ESI† for isolated yield determination and NMR spectra).

Reaction 2. In dry glassware 1,3,5-trimethoxybenzene, sodium trifluoromethylsulfinate (4 eq), and 4:1 mixture of ethyl acetate and diacetyl were added. To this mixture, nitrogen gas was sparged at 0 °C for 15 min. The glassware was made air-tight and put into the irradiation module. The reactor was set to the desired voltage and electrical current. The flow rate of the pump was also set as needed. 5 μL

2220 | *React. Chem. Eng.*, 2023, **8**, 2211–2222

This journal is © The Royal Society of Chemistry 2023

reaction mixture was taken and diluted to 1000 μL for each sampling. The sampling was done between 5 min time intervals. The yield was measured with respect to the previously determined standard curve by using a known concentration of 1,3,5-trimethoxybenzene in HPLC.

The reaction mixture collected from the reactor was filtered by using Whatman filter paper. The white color residue was washed using ethyl acetate and then hexane. Then the solvent was evaporated and the crude product was purified by column chromatography. The product was synthesized and separated according to the reported procedure and the spectroscopic data are in agreement with the literature[50] (please see page 32 of the ESI† for isolated yield determination and NMR spectra).

Author contributions

Shibu Naskar and Daniel Kowalczyk have contributed equally towards conceptualization, data curation, formal analysis, investigation, methodology, project administration, software, validation, visualization, writing of the original draft and review and editing of the manuscript and ESI.† Photoreactor manufacturing, photoreactions and analytics were performed at the National Institute of Technology Patna and the National Institute of Pharmaceutical Education and Research Hajipur. The photonic characterization of the light sources and the evaluation of the used setup and the experimental data of the photoreactions were conducted at the Institute of Chemical Engineering at Ulm University. Susital Mal supported with data curation, formal analysis, investigation and validation of experimental and analytical results. Subrata Das and Dirk Ziegenbalg have contributed equally towards conceptualization, funding acquisition, resources, overall supervision, review and editing of the write-up of the main manuscript and ESI.† Prakash Kumar & Debabrata Mandal have contributed support towards investigation, data curation and formal analysis (HPLC analysis).

Conflicts of interest

There are no conflicts to declare.

Acknowledgements

References

1 M. H. Shaw, J. Twilton and D. W. C. MacMillan, *J. Org. Chem.*, 2016, **81**, 6898–6926.

2 J. Twilton, C. C. Le, P. Zhang, M. H. Shaw, R. W. Evans and D. W. C. MacMillan, *Nat. Rev. Chem.*, 2017, **1**, 52.

3 M. D. Kärkäs, J. A. Porco and C. R. J. Stephenson, *Chem. Rev.*, 2016, **116**, 9683–9747.

4 N. A. Romero and D. A. Nicewicz, *Chem. Rev.*, 2016, **116**, 10075–10166.

5 C. K. Prier, D. A. Rankic and D. W. C. MacMillan, *Chem. Rev.*, 2013, **113**, 5322–5363.

6 K. L. Skubi, T. R. Blum and T. P. Yoon, *Chem. Rev.*, 2016, **116**, 10035–10074.

7 K. Teegardin, J. I. Day, J. Chan and J. Weaver, *Org. Process Res. Dev.*, 2016, **20**, 1156–1163.

8 L. D. Elliott, J. P. Knowles, P. J. Koovits, K. G. Maskill, M. J. Ralph, G. Lejeune, L. J. Edwards, R. I. Robinson, I. R. Clemens, B. Cox, D. D. Pascoe, G. Koch, M. Eberle, M. B. Berry and K. I. Booker-Milburn, *Chem. – Eur. J.*, 2014, **20**, 15226–15232.

9 J. W. Beatty, J. J. Douglas, K. P. Cole and C. R. J. Stephenson, *Nat. Commun.*, 2015, **6**, 6–11.

10 C. C. Le, M. K. Wismer, Z. C. Shi, R. Zhang, D. V. Conway, G. Li, P. Vachal, I. W. Davies and D. W. C. MacMillan, *ACS Cent. Sci.*, 2017, **3**, 647–653.

11 M. B. Plutschack, B. Pieber, K. Gilmore and P. H. Seeberger, *Chem. Rev.*, 2017, **117**, 11796–11893.

12 D. Cambié, C. Bottecchia, N. J. W. Straathof, V. Hessel and T. Noël, *Chem. Rev.*, 2016, **116**, 10276–10341.

13 B. Wriedt, D. Kowalczyk and D. Ziegenbalg, *ChemPhotoChem*, 2018, **2**, 913–921.

14 O. Shvydkiv, S. Gallagher, K. Nolan and M. Oelgemöller, *Org. Lett.*, 2010, **12**, 5170–5173.

15 Z. Dong, Z. Wen, F. Zhao, S. Kuhn and T. Noël, *Chem. Eng. Sci.: X*, 2021, **10**, 100097.

16 L. Buglioni, F. Raymenants, A. Slattery, S. D. A. Zondag and T. Noël, *Chem. Rev.*, 2022, **122**, 2752–2906.

17 B. D. A. Hook, W. Dohle, P. R. Hirst, M. Pickworth, M. B. Berry and K. I. Booker-Milburn, *J. Org. Chem.*, 2005, **70**, 7558–7564.

18 L. D. Elliott, M. Berry, B. Harji, D. Klauber, J. Leonard and K. I. Booker-Milburn, *Org. Process Res. Dev.*, 2016, **20**, 1806–1811.

19 Y. Su, N. J. W. Straathof, V. Hessel and T. Noël, *Chem. – Eur. J.*, 2014, **20**, 10562–10589.

20 K. C. Harper, E. G. Moschetta, S. V. Bordawekar and S. J. Wittenberger, *ACS Cent. Sci.*, 2019, **5**, 109–115.

21 A. Chaudhuri, K. P. L. Kuijpers, R. B. J. Hendrix, P. Shivaprasad, J. A. Hacking, E. A. C. Emanuelsson, T. Noël and J. van der Schaaf, *Chem. Eng. J.*, 2020, **400**, 125875.

22 D. S. Lee, Z. Amara, C. A. Clark, Z. Xu, B. Kakimpa, H. P. Morvan, S. J. Pickering, M. Poliakoff and M. W. George, *Org. Process Res. Dev.*, 2017, **21**, 1042–1050.

23 D. S. Lee, M. Sharabi, R. Jefferson-Loveday, S. J. Pickering, M. Poliakoff and M. W. George, *Org. Process Res. Dev.*, 2020, **24**, 201–206.

This journal is © The Royal Society of Chemistry 2023

React. Chem. Eng., 2023, **8**, 2211–2222 | **2221**

24 D. Ziegenbalg, P. Löb, M. Al-Rawashdeh, D. Kralisch, V. Hessel and F. Schönfeld, *Chem. Eng. Sci.*, 2010, **65**, 3557–3566.

25 D. C. Fabry, Y. A. Ho, R. Zapf, W. Tremel, M. Panthöfer, M. Rueping and T. H. Rehm, *Green Chem.*, 2017, **19**, 1911–1918.

26 S. Schlögl, A. Temel, R. Schaller, A. Holzner and W. Kern, *J. Appl. Polym. Sci.*, 2012, **124**, 3478–3486.

27 K. H. Hama Aziz, *Chemosphere*, 2019, **228**, 377–383.

28 W. Lou, A. Kane, D. Wolbert, S. Rtimi and A. A. Assadi, *Chem. Eng. Process.*, 2017, **122**, 213–221.

29 G. L. Puma and P. L. Yue, *Environ. Sci. Technol.*, 1999, **33**, 3210–3216.

30 O. M. Alfano, D. Bahnemann, A. E. Cassano, R. Dillert and R. Goslich, *Catal. Today*, 2000, **58**, 199–230.

31 D. Ziegenbalg, A. Pannwitz, S. Rau, B. Dietzek-Ivanšić and C. Streb, *Angew. Chem., Int. Ed.*, 2022, **61**, 1–11.

32 D. Ziegenbalg, A. Pannwitz, S. Rau, B. Dietzek-Ivanšić and C. Streb, *Angew. Chem., Int. Ed.*, 2022, **61**, e202114106.

33 D. Ziegenbalg, B. Wriedt, G. Kreisel and D. Kralisch, *Chem. Eng. Technol.*, 2016, **39**, 123–134.

34 H. Raach, *Falling Film. Desalin.*, 2019, pp. 41–64.

35 G. Ritzoulis, N. Papadopoulos and D. Jannakoudakis, *J. Chem. Eng. Data*, 1986, **31**, 146–148.

36 S. S. Arbuj, S. B. Waghmode and A. V. Ramaswamy, *Tetrahedron Lett.*, 2007, **48**, 1411–1415.

37 P. Ghosh and P. S. Mitra, *J. Polym. Sci., Polym. Chem. Ed.*, 1976, **14**, 993–1004.

38 P. K. Chhattise, A. V. Ramaswamy and S. B. Waghmode, *Tetrahedron Lett.*, 2008, **49**, 189–194.

39 D. A. Rogers, R. G. Brown, Z. C. Brandeburg, E. Y. Ko, M. D. Hopkins, G. Leblanc and A. A. Lamar, *ACS Omega*, 2018, **3**, 12868–12877.

40 D. Cantillo, O. De Frutos, J. A. Rincon, C. Mateos and C. Oliver Kappe, *J. Org. Chem.*, 2014, **79**, 223–229.

41 K. Müller, C. Faeh and F. Diederich, *Science*, 2007, **317**, 1881–1886.

42 W. K. Hagmann, *J. Med. Chem.*, 2008, **51**, 4359–4369.

43 Y. Zhou, J. Wang, Z. Gu, S. Wang, W. Zhu, J. L. Acenã, V. A. Soloshonok, K. Izawa and H. Liu, *Chem. Rev.*, 2016, **116**, 422–518.

44 C. Alonso, E. Martínez De Marigorta, G. Rubiales and F. Palacios, *Chem. Rev.*, 2015, **115**, 1847–1935.

45 O. A. Tomashenko and V. V. Grushin, *Chem. Rev.*, 2011, **111**, 4475–4521.

46 D. J. Burton and Z. Y. Yang, *Tetrahedron*, 1992, **48**, 189–275.

47 T. Furuya, A. S. Kamlet and T. Ritter, *Nature*, 2011, **473**, 470–477.

48 E. J. Cho, T. D. Senecal, T. Kinzel, Y. Zhang, D. A. Watson and S. L. Buchwald, *Science*, 2010, **328**, 1679–1681.

49 X. Wang, L. Truesdale and J. Q. Yu, *J. Am. Chem. Soc.*, 2010, **132**, 3648–3649.

50 L. Li, X. Mu, W. Liu, Y. Wang, Z. Mi and C. J. Li, *J. Am. Chem. Soc.*, 2016, **138**, 5809–5812.

51 M. Sender and D. Ziegenbalg, *React. Chem. Eng.*, 2021, **6**, 1614–1627.

2222 | *React. Chem. Eng.*, 2023, **8**, 2211–2222

This journal is © The Royal Society of Chemistry 2023